Hamburger Beiträge
zur Angewandten Mathematik

Proper Orthogonal Decomposition for Free Boundary Value Problems

Michael Hinze, Joachim Krenciszek, and René Pinnau

Nr. 2014-17
September 2014

Proper **O**rthogonal **D**ecomposition for Free Boundary Value Problems

Michael Hinze[†], Joachim Krenciszek[*], and René Pinnau[*]

September 19, 2014

Abstract

We use the method of proper orthogonal decomposition for the derivation of surrogate models for free boundary value problems. Exemplarily, we study a single-phase Stefan problem in one spatial dimension and a two-phase Stefan problem in two dimensions. For the first one we use three different numerical approaches to treat the moving free boundary for the calculation of the snapshots and compare the performance of the reduced models. In the second problem we use a fixed grid approach and simulate the apparent heat equation. In all cases we provide numerical examples underlining the feasibility of our approach and we present studies on the robustness of the reduced surrogate models with respect to changes in the data.

Keywords Free Boundary Value Problem, Stefan Condition, Proper Orthogonal Decomposition, Surrogate Models, Robustness

MSC (2010) 35R35, 65N30

1 Introduction

The increasing complexity of models for industrial applications in combination with the requirement of faster simulation times makes the usage of modern model reduction techniques mandatory. During the last decades proper orthogonal decomposition (POD) proved to be a reliable tool for the reduction of nonlinear partial differential equations [21].

Proper orthogonal decomposition is a method to determine an optimal subspace basis, similar to the concepts of Karhunen-Loève expansion and principal component analysis. Applied as a method of model reduction, the data that is approximated in an optimal least square sense is given in the form of solutions of the full systems or can even be obtained from experimental measurements. As a purely data-driven method POD can also be used as a data analysis method and has been used in the analysis of turbulence and coherent structures in fluid dynamics [3, 4, 17, 22, 26, 27], the same application for which model reduction with POD was first studied. It was successfully applied to optimal control problems of partial differential equations [2, 7, 8, 12, 13, 24] and simulation of integrated circuits [11, 23]. Recently, POD is applied to inverse problems in structural mechanics [5] and used to set up low-dimensional

[*]Fachbereich Mathematik, Technische Universität Kaiserslautern, D-67663 Kaiserslautern, Germany
[†]Fachbereich Mathematik, Universität Hamburg, D-20146 Hamburg, Germany

surrogate models for application in durability analysis and optimal design [1,9,10,15,18]. For a detailed overview and a classical application example of POD in a nonlinear radiative heat transport problem see [21].

Here, we are going to consider POD for free boundary value problems, in particular a single-phase Stefan problem in one spatial dimension and a two-phase Stefan problem in two dimensions. This problem class is interesting due to the high nonlinearity and some challenging numerical issues coming from the resolution of the evolution of the free boundary.

First, we consider the single-phase Stefan problem which describes the temperature distribution in a homogeneous medium undergoing a phase change, e.g., a melting block of ice. Modelled as a free boundary problem on a semi infinite domain, the interval $[0, s(t)]$ is occupied by water and increases in size as the heat flux at the boundary $s(t)$ causes a melt down. Since we neglect heat sources and have zero Dirichlet boundary conditions, the melt down process is governed by the initial temperature distribution. The precise mathematical formulation reads:

Find a pair $(u(x,t), s(t))$ that satisfies the system:

$$
\begin{aligned}
&u_t - \kappa u_{xx} = 0 && \text{in } \{(x,t) : 0 < x < s(t), 0 < t < T_0\}, && \text{(heat equation)}\\
&u(x,0) = f(x) && \text{for } x \text{ in } (0,1), && \text{(initial temperature)}\\
&u(0,t) = 0 && \text{for } 0 \le t \le T_0 && \\
&u(s(t),t) = 0 && \text{for } 0 \le t \le T_0 && \\
&s_t + \kappa u_y(s(t),t) = 0 && \text{for } 0 < t \le T_0 && \text{(Stefan condition)}\\
&s(0) = 1 &&&&
\end{aligned}
\tag{1.1}
$$

Here, $\kappa > 0$ denotes the diffusion coefficient and $f \ge 0$ denotes an initial condition which satisfies $f(0) = f(1) = 0$.

For this problem we are going to use three different numerical approaches for the simulation from which we extract the snapshots for the construction of the reduced POD basis. First, we consider a Landau-type transformation which allows for the transformation on a fixed spatial domain. Second, we provide a fixed grid on a larger interval in which the free boundary is moving. Lastly, the grid is moving and stretched according to the evolution of the free boundary. While the first approach is restricted to one spatial dimension, the other two can be easily generalized to higher dimensions.

In two spatial dimensions we are going to simulate the temperature distribution $u(x,t)$ in two different media with different specific heat capacities, heat conductivities and densities separated by a free boundary which evolves according to a Stefan condition (see Figure 1). The problem reads: Find $u(x,t)$ and $f(x,t)$ such that

$$
\begin{aligned}
\operatorname{div}(\kappa_s \nabla u) &= \rho_s c_s \, \partial_t u && (x,t) \in \Omega_s \times (0,T)\\
\operatorname{div}(\kappa_l \nabla u) &= \rho_l c_l \, \partial_t u && (x,t) \in \Omega_l \times (0,T)\\
u(x,0) &= u_0(x) && x \in \Omega_s \cup \Omega_l\\
u(x,t) &= u_b(x,t) && (x,t) \in \partial(\Omega_s \cup \Omega_l) \times (0,T)
\end{aligned}
$$

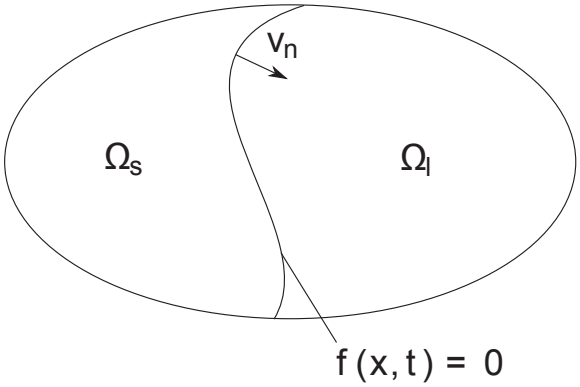

Figure 1: Two-phase region with moving boundary $f(x,t) = 0$

as well as

$$\rho L v_n = \kappa_s \frac{\partial u_s}{\partial n} - \kappa_l \frac{\partial u_l}{\partial n} \tag{1.2}$$

on the free boundary $f(x,t) = 0$.

Density, heat conductivity and heat capacity of the solid and liquid media are positive constants denoted by ρ_s, ρ_l, κ_s and κ_l, c_s, c_l, respectively. The constant L is the latent heat, which is the heat absorbed or released during a phase transition that occurs without a change of temperature. Further, v_n is the normal velocity of the free boundary.

As shown in [25], this problem can be reformulated to the enhanced or apparent heat capacity equation

$$c^A \partial_t u = \operatorname{div}(\kappa \nabla u), \tag{1.3}$$

where

$$c^A = g_s \rho_s c_s + g_l \rho_l c_l + ((\rho_l c_l - \rho_s c_s)(u - u_{ref}) + \rho_l L) \frac{dg_l}{du}$$

and

$$\kappa = g_l \kappa_l + g_s \kappa_s.$$

Here, $g_l = g_l(u)$ is the liquid volume fraction (see e.g. [25]), $g_s = 1 - g_l$ the solid volume fraction and u_{ref} is an arbitrary reference temperature. Now the equation is in a form which allows for a simulation on a fixed grid. But one has to pay the price that the apparent heat capacity strongly depends on space and time. Nevertheless, this formulation is now adequate for the direct application of POD.

The paper is organized as follows. In Section 2 we briefly review the method of proper orthogonal decomposition based on snapshots. Section 3 is devoted to the study of the single-phase Stefan problem. We use the three different methods for the calculation of the snapshots, compare the performance of reduced the POD models and study their robustness with respect to changes in the data. Finally, we present in Section 4 a fixed grid approach for the apparent heat equation modelling a two-phase Stefan problem in two dimensions, employ POD and study again the robustness of the surrogate model. Concluding remarks are given in Section 5.

2 Proper Orthogonal Decomposition

In the following we shortly review the standard snapshot POD approach, for a detailed description we refer to [12, 21].

Let $(X, (\cdot,\cdot))$ denote a Hilbert space, and let $y_1, \dots, y_m \in X$ denote vectors which are obtained e.g. from a numerical simulation of a dynamical system as time snapshots $y_i \equiv y(t_i)$, or from an experiment (y_i denotes the $i-$th sample or snapshot of the experiment). The snapshots are stored in the snapshot matrix

$$Y = [y_1, \dots, y_m] \in X^m. \tag{2.1}$$

The POD approach now seeks for an orthonormal basis $\{\varphi_i \mid i = 1, \dots, l\}$ of rank $1 \le l \le \dim\{Y\}$ which carries as much information as possible contained in Y w.r.t. the inner product $(\cdot,\cdot)$, i.e.

$$\{\varphi_i \mid i = 1, \dots, l\} = \underset{(\varphi_l,\varphi_k)=\delta_{lk}}{\arg\min} \sum_{i=1}^{m} \|y_i - \sum_{j=1}^{l} (y_i, \varphi_j)\varphi_j\|^2, \tag{2.2}$$

where $\|\cdot\| := (\cdot,\cdot)^{1/2}$.

The solution to this minimization problem is called *POD basis of rank l*, and is given by

$$\varphi_i = \frac{1}{\sqrt{\lambda_i}} Y v^i \quad (i = 1, \dots, l),$$

with $v^i \in \mathbb{R}^m$ denoting the $i-$th eigenvector of $(Y,Y) \in \mathbb{R}^{m,m}$ with eigenvalue $\lambda_i \ge 0$. The minimal projection error can then be expressed in terms of the omitted eigenvalues λ_i, i.e.

$$\min_{\varphi_j} \sum_{i=1}^{n} \|y_i - \sum_{j=1}^{l} \langle y_i, \varphi_j\rangle \varphi_j\|^2 = \sum_{i=l+1}^{m} \lambda_i \ . \tag{2.3}$$

2.1 Reduced Order Modeling of a Semilinear Evolution Problem

Now we briefly sketch how the POD method is applied to obtain reduced order dynamics for abstract semilinear evolution equations of the form

$$\partial_t y = Ay + b(t, y) \text{ in } (0, T], \tag{2.4}$$

$$y(0) = y_0, \tag{2.5}$$

where $T > 0$, $A : V \to V'$ denotes a coercive operator, $b : (0, T] \times V \to V'$ an appropriate nonlinearity, and $y_0 \in H$ the initial value. Here, (V, H, V') denotes a Gelfand triple, so that in the following we can choose $X = H$ or $X = V$. To simplify the exposition we from here onwards choose $X = H$.

From the numerical simulation of (2.4) at time instances t_i $(i = 1, \dots, m)$ we obtain snapshots $y_1, \dots, y_m \in X$, for which we compute the POD basis $\{\varphi_1, \cdots, \varphi_l\}$ of rank l according to (2.2). We define $\Phi = [\varphi_1, \dots, \varphi_l] \in X^m$ and make the ansatz

$$y^l(t) := \sum_{j=1}^{l} \alpha_j(t)\varphi_j \equiv \Phi\alpha(t). \tag{2.6}$$

We insert the ansatz into (2.4) and test the resulting system with the POD basis. This POD Galerkin scheme delivers the reduced IVP in l variables;

$$\begin{aligned} \dot{\alpha} &= \tilde{A}\alpha + \tilde{b}(t, \Phi\alpha), \\ \alpha(0) &= (\Phi, y_0)^t, \end{aligned}$$

where

$$\tilde{A} = \langle A\Phi, \Phi\rangle_{V'V}, \quad \tilde{b}(t,\alpha) = \langle b(t,\Phi\alpha), \Phi\rangle_{V'V}, \text{ and } \quad (\Phi, y_0) := ((\varphi_1, y_0), \ldots, (\varphi_l, y_0)).$$

3 The Single-Phase Stefan Problem in One Dimension

Problem (1.1) is difficult to tackle with common POD techniques since the spatial domain is time-dependent, i.e., it depends on the position of the free boundary $s(t)$. In the following we consider three approaches to overcome this difficulty and to make POD applicable.

3.1 The Landau Transformation

First, we transform (1.1) using the following Landau-type transformation, as described in [20],

$$x = s(t)y \qquad \text{and} \qquad \tau = \int_0^t \frac{1}{s(k)^2} dk \ .$$

After a short computation we find that $U(y,\tau) := u(x,t)$ satisfies the nonlinear parabolic equation

$$\begin{aligned} &U_\tau(y,\tau) - \kappa U_{yy}(y,\tau) = -\kappa U_y(1,\tau) y U_y(y,\tau) \\ &\text{in } \{(y,\tau) : y \in (0,1), 0 < \tau \le T\} \\ &\\ &U(0,\tau) = U(1,\tau) = 0 \qquad\qquad \text{for } \tau > 0 \\ &U(y,0) = f(y) \qquad\qquad \text{for } y \in (0,1) \end{aligned} \tag{3.1}$$

and the boundary position $S(\tau) = s(t)$ of the free boundary is determined by

$$\begin{aligned} &S_\tau(\tau) = -\kappa U_y(1,\tau) S(\tau) \qquad \text{for } \tau > 0, \quad S(0) = 1 \\ &t_\tau = S^2(\tau) \qquad\qquad \text{with } t(0) = 0 \ . \end{aligned} \tag{3.2}$$

We note that (3.1) does not depend on S, so that the position of the free boundary can be calculated using (3.2) once U is known from (3.1).

Since (3.1) forms a nonlinear parabolic equation, it can be approximated by a Galerkin method based on the POD modes obtained from the snapshots. The Galerkin solution then can be used to form the mobility of S in (3.2) and to compute the approximate position of the free boundary.

3.1.1 Numerical Solution and POD Reduction

For the numerical approximation of (3.1) we use linear finite elements on the equidistant grid $x_i := \frac{i}{n+1}$, $i = 0, \ldots, n+1$. The resulting nonlinear system of ODEs then reads

$$M\dot{U} = \kappa KU - \kappa F(U) \ , \tag{3.3}$$

where M is the mass matrix, K is the stiffness matrix and the nonlinearity F has the form

$$F(U) := \frac{1}{4} U_n T U, \quad \text{with} \quad T := \begin{pmatrix} -2 & 3 & & & & \\ -3 & -2 & 5 & & & \\ & \ddots & \ddots & \ddots & & \\ & & -(2n-3) & -2 & 2n-1 & \\ & & & & -(2n-1) & -2 \end{pmatrix}, \tag{3.4}$$

where we use the element-wise midpoint rule to numerically integrate the terms $\int_\Omega y U_y \phi_j dy$ with FE hat functions ϕ_j, for $j = 1, \ldots, n$.

This ODE system can be solved with standard algorithms such that we can build up the snapshot matrix $Y = [U(t_0), \ldots, U(t_m)]$. We set $X := \mathbb{R}^n$ equipped with the Euclidean scalar product. The POD basis $\Phi = [\varphi_1, \ldots, \varphi_l] \in \mathbb{R}^{n,m}$ obtained from Y in this setting is now used to create a reduced order model of (3.3). It reads

$$\tilde{M}\dot{\tilde{U}} = \kappa \tilde{K}\tilde{U} - \kappa \tilde{F}(\tilde{U}), \tag{3.5}$$

where $\tilde{M} := \Phi^T M \Phi$, $\tilde{K} := \Phi^T K \Phi$ and

$$\tilde{F}(\tilde{U}) := \frac{1}{4} \left(\sum_{i=1}^{l} \varphi_i^n \tilde{U}_i \right) \tilde{T}\tilde{U} \quad \text{with } \tilde{T} := \Phi^T T \Phi. \tag{3.6}$$

Once the reduced solution is computed, the motion of the boundary $\tilde{S}$ can be obtained from

$$\begin{aligned} &\tilde{S}_\tau(\tau) = -\kappa(n+1) \left(\sum_{i=1}^{l} \varphi_i^n \tilde{U}_i \right) \tilde{S}(\tau) && \text{for } \tau > 0, \quad \tilde{S}(0) = 1 \\ &t_\tau = \tilde{S}^2(\tau) && \text{with } t(0) = 0 \ . \end{aligned} \tag{3.7}$$

3.2 The Control Volume Approach

For the second numerical approach we start with a spatial discretization of a larger domain $\bar{\Omega} = (0, S_0)$, assuming the free boundary will not leave this domain in the regarded time interval, i.e., $s(t) < S_0$, for all $t < T_0$. The heat equation part of (1.1) is solved using linear finite elements on the part of the grid that is still confined by the free boundary $s(t)$. This implies that M and K have to be updated each time $s(t)$ passes a new grid point.

Let $0 \leq t_{p1} \leq \cdots \leq t_{p_{mp}} \leq T_0$ be the points in time when the moving boundary passes a new grid point. Then we use the following numerical procedure:
Algorithm:

- solve $M(p_i)\dot{u} = \kappa K(p_i)u$ in $(t_{p_i}, t_{p_{i+1}})$
- project solution to original grid
- add new cell with melting point temperature
- project solution back to reference grid
- update mass and stiffness matrix and continue simulation

To determine $t_{p_{i+1}}$ we update $s(t)$ by the temperature at the last active grid point using the Stefan condition from (1.1) and determine the phase change at the next grid point. New grid points are initialized with zero temperature when joining the active domain $\Omega = (0, s(t))$.

Remark 3.1 *Unlike the method presented in the previous section, this approach can easily be generalized to higher dimensions or different types of boundary conditions. But the computational costs increase as mass and stiffness matrices grow during the simulation.*

3.2.1 POD Reduction

Since the length of the snapshots changes during the simulation, POD cannot be applied in a straightforward manner. First, we have to map all snapshots by rescaling and interpolation back to the interval $\bar{\Omega}$. From this projected snapshot matrix we compute the POD basis.

During the numerical approximation, each time the free boundary s passes a new grid point, we have to map U to the full space using Φ, rescale and interpolate back to the active domain Ω, add a zero temperature entry for the new grid point and finally project back to the POD space via the reference grid $\bar{\Omega}$. For a overview of the algorithm see the flowchart in Figure 2.

3.3 The Moving Mesh Approach

In this last approach we keep the number of grid points fixed but move them with regard to the evolution of the free boundary $s(t)$. To guarantee the conservation of energy, the temperature at the new grid points has to be interpolated with respect to the new grid, as is sketched in Figure 3. The movement of the grid points is governed by the the ODE

$$\dot{x_i} = \dot{s}\,\frac{i}{n+1}. \tag{3.8}$$

If we assume that s is monotonically increasing and Δt is small enough such that s does not exceed more than one grid point in one time step, then the projection reads

$$\bar{u_i} = u_i\left(1 - \frac{\dot{x_i}\Delta t}{\Delta x}\right) + u_{i+1}\frac{\dot{x_i}\Delta t}{\Delta x}. \tag{3.9}$$

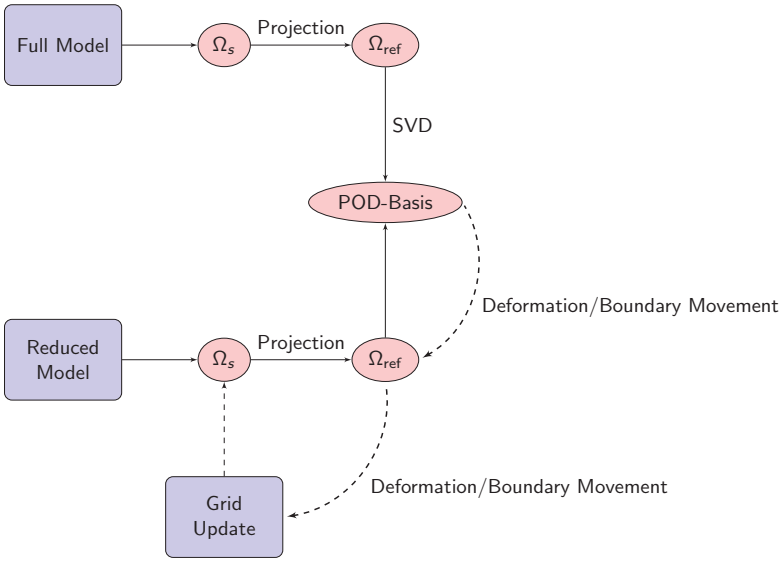

Figure 2: POD reduced model using a fixed grid method

In the limit $\Delta t \to 0$ this can be expressed as

$$\dot{u}_i = (u_{i+1} - u_i)\frac{\dot{s}}{s} i \ . \tag{3.10}$$

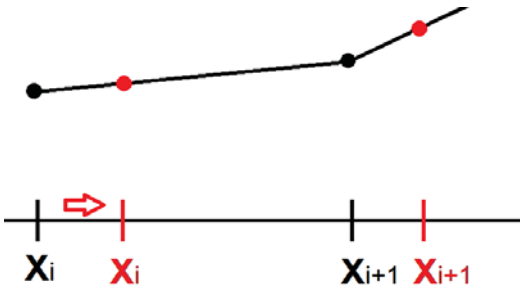

Figure 3: Grid update for the moving mesh method

Incorporating this projection term into the ODE from the FE ansatz we obtain

$$\dot{u} = \kappa M^{-1} K u + R u \frac{\dot{s}}{s} = \kappa \left(M^{-1} K u + R u \frac{u_n(n+1)}{s^2} \right) \tag{3.11}$$

$$\dot{s} = \kappa \frac{u_n(n+1)}{s} \ , \tag{3.12}$$

$$\text{with} \quad R := \begin{pmatrix} -1 & 1 & & & & \\ & -2 & 2 & & & \\ & & \ddots & \ddots & & \\ & & & -(n-1) & (n-1) & \\ & & & & -n & \end{pmatrix} . \tag{3.13}$$

Remark 3.2 *Note, that the mass matrix M and the stiffness matrix K depend on s, but since we use equidistant finite linear elements they can be written as $M(s) = \frac{n+1}{s} M_0$ and $K(s) = \frac{n+1}{s} K_0$, where M_0 and K_0 are constant matrices.*

Now, we can directly apply POD, but as in the previous sections it should only be applied to the temperature u, i.e., the position of the free boundary is not incorporated into the snapshots and dealt with separately.

The reduced model then reads

$$\dot{\tilde{u}} = \kappa \Phi^T M^{-1} K \Phi \tilde{u} + \Phi^T R \Phi \tilde{u} \frac{\dot{\tilde{s}}(t)}{\tilde{s}(t)}$$

$$\dot{\tilde{s}} = \kappa \frac{(n+1)}{\tilde{s}} \left(\sum_{i=1}^{l} \varphi_i^n \tilde{u}_i \right) .$$

3.4 Numerical Comparison of the Three Approaches

The approximation quality of the reduced systems is linked to the accuracy of the position of the free boundary which is measured by

$$\int_0^{T_0} |s(t) - \tilde{s}(t)|^2 dt \tag{3.14}$$

and will be the main criterion in comparing the different reduced models.

For the numerical example we choose $T_0 = 20$, $\kappa = 0.1$, $n = 500$, and $f(x) = 4x(1-x)$ for $x \in (0,1)$. In all cases, 100 equidistant snapshots are used to form the correlation matrix Y. For time integration, an adaptive step size control with both relative and absolute tolerances of 10^{-8} is used for all three methods.

In Figure 4(a) one finds the eigenvalues of the correlation matrix calculated from the snapshots of the first approach. For the other two methods there is no significant difference and the overall behaviour suggests that one can expect a good approximation property of the reduced POD model in view of Eq. (2.3). Figure 4 and 5 show that for the Landau-type

transformation and the moving mesh approach the reduced models give already good results for very few modes. But the reduced model of the control volume approach does not yield a good approximation quality until at least 10 modes. Further, we see in Figure 5 that the error stagnates at a rather rough level compared to the other two approaches. However, the other two methods show steady improvement of the approximation quality. An explanation for the worse behaviour of the second method might be the projection step in the algorithm (see also Figure 2), which introduces an additional error.

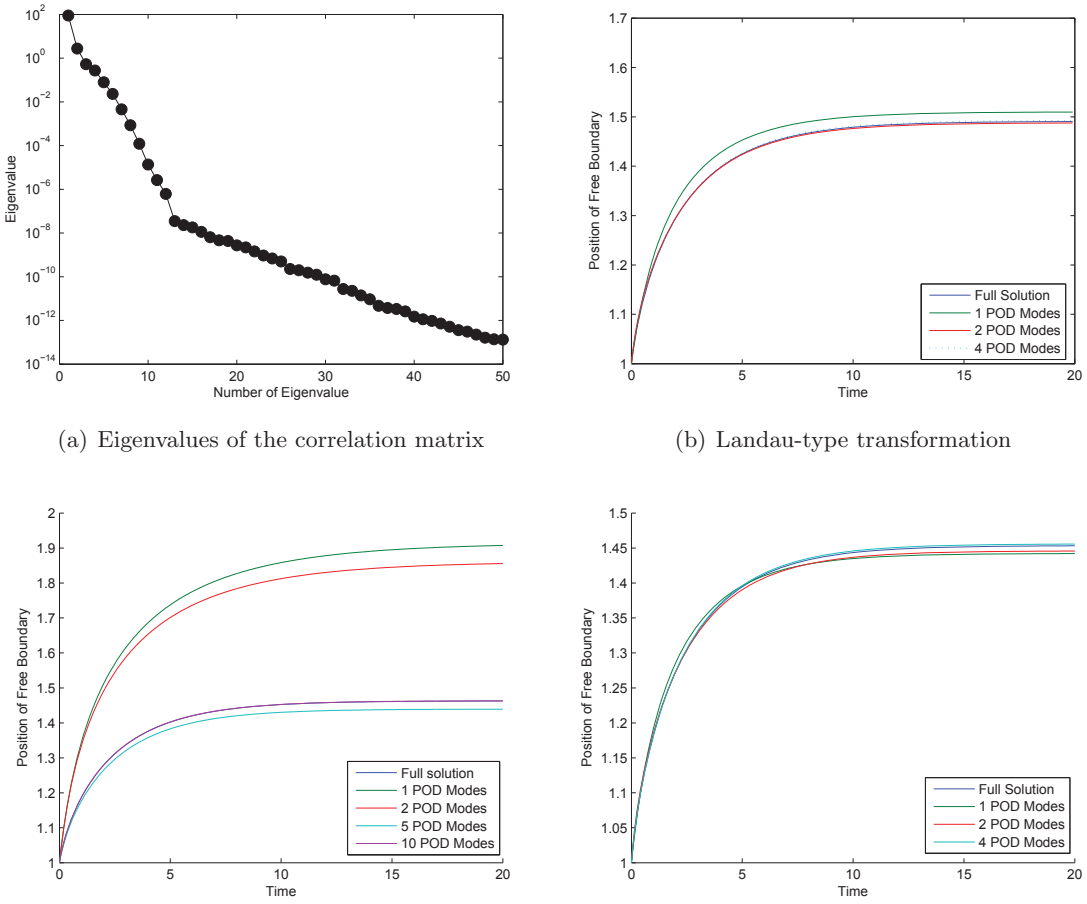

(a) Eigenvalues of the correlation matrix

(b) Landau-type transformation

(c) Control Volume

(d) Moving Mesh

Figure 4: Position of the free boundary $s(t)$ for the different POD reduced models

3.4.1 Sensitivities and Robustness

Next, we investigate the robustness of the reduced POD model with respect to changes in the data for the simulation. Since the behavior depends critically on the parameter κ, we present first results for the different values $\kappa = 0.01$ and $\kappa = 1$ in the reduced model, while the POD basis is constructed from the simulation with $\kappa = 0.1$. In the latter case we choose $T_0 = 5$, because the melting process happens much faster. As can be seen in Figure 6 similar results

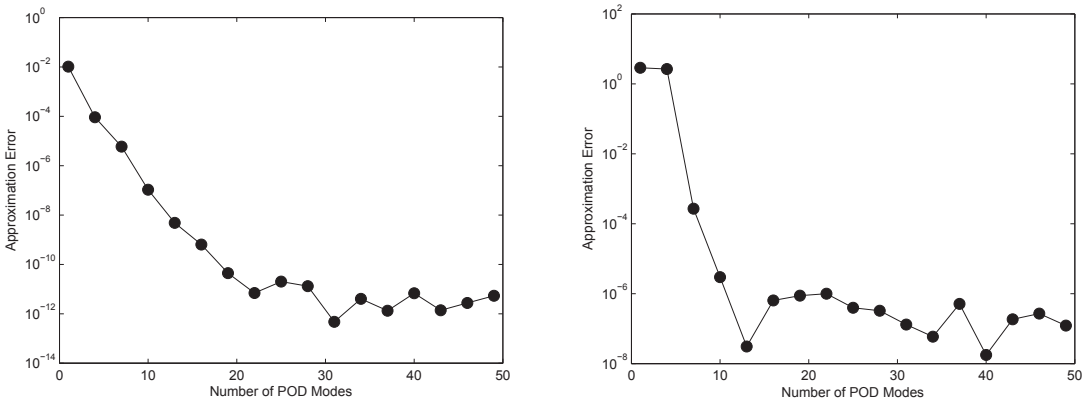

(a) Landau-type transformation

(b) Control Volume

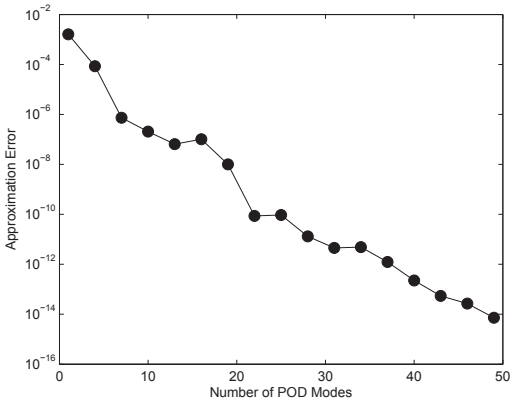

(c) Moving Mesh

Figure 5: Approximation error of the POD reduced systems

can be achieved and there is no strong sensitivity on κ.

Second, to avoid time-consuming simulations of the full system to generate the snapshots for the POD basis we investigate the quality of the reduced systems gained from only 100 snapshots from the first second ($T_0 = 1$). The results in Figure 7 show that the relevant dynamics can be captured in the POD-basis even if only the first second of the full system is used to generate snapshots.

Lastly, to test the reduced model for robustness with respect to changes in the initial data, we generate the snapshots using modified initial condition $f(x) = \sqrt{4x(1-x)}$. As can be seen in Figure 8, all three methods show again a robust behaviour also regarding this change.

4 Two-Phase Stephan Problem

In this section we study the two-phase Stefan problem in two spatial dimensions modelled by the apparent heat equation (1.3). This form is identical to the basic Fourier heat conduction equation, but the apparent heat capacity c^A as well as the heat conductivity κ are highly dependent on space and time. Since the domain is fixed, we can generate a mesh and use linear finite elements in space yielding a nonlinear dynamical system of the form

$$M(u)\dot{u} + K(u)u = b. \tag{4.1}$$

The mass matrix M and the stiffness matrix K depend on the temperature distribution u, because c^A and k are temperature dependent. Since the element mass and stiffness matrices are constant, except for a small region around the free boundary, we update the full matrices only by applying the changes to the corresponding element matrices. The change of the i-th element mass matrix is given by

$$\triangle M_{ei} = \triangle c_i^A \cdot J_i \frac{1}{24} \begin{pmatrix} 2 & 1 & 1 \\ 1 & 2 & 1 \\ 1 & 1 & 2 \end{pmatrix},$$

and the change of the i-th element stiffness matrix is just

$$\triangle K_{ei} = \triangle \kappa_i \cdot \frac{1}{2J_i} A^T A,$$

where $\triangle$ indicates the change from the previous time step, J_i is the surface area of the i-th patch and A is given by

$$A = \begin{pmatrix} y_2 - y_3 & y_3 - y_1 & y_1 - y_2 \\ x_3 - x_2 & x_1 - x_3 & x_2 - x_1 \end{pmatrix},$$

with $(x_k, y_k),\ k = 1, 2, 3$ the coordinates of the i-th face. This procedure allows us to update the mass and stiffness matrix in an optimal way and avoids rebuilding of the matrices.

4.1 Numerical Results

Next, we apply POD to the two-phase Stefan problem on a rectangular domain with a circular hole. The material properties ρ, c and κ are chosen for water and ice (see Table 1).

material property	solid	liquid
$\rho\ (kg/m^3)$	920 000	1000 000
$c\ (J/(kg \cdot K))$	2060	4200
$\kappa\ (W/(m \cdot K))$	2.33	0.5562

Table 1: Material Parameters

Initially, the whole domain is full of ice at a temperature of $-2\,^{\circ}\mathrm{C}$, which is heated by a constant temperature of $20\,^{\circ}\mathrm{C}$ from the boundary (outer rectangle and inner circle). The liquid volume fraction is modelled by

$$g_l(u) = \begin{cases} 0, & u < T_\epsilon \\ \epsilon_S + \frac{1-\epsilon_L-\epsilon_S}{T_L-T_\epsilon} \cdot (u - T_\epsilon), & T_\epsilon \le u \le T_L \\ 1, & T_L < u \end{cases},$$

where ϵ_S and ϵ_L describe the step discontinuity due to the phase change at the mush/solid interface with freezing point T_S and melting point T_L.

The original problem is discretized using linear finite elements, yielding a ODE system with 37659 degrees of freedom. Figure 9 shows the melting of the ice cube and the temperature distribution inside the solid medium at four different points in time.

After projection to the POD basis the reduced Model reads

$$\Phi^T M(\Phi\tilde{u})\Phi\dot{\tilde{u}} + \Phi^T K(\Phi\tilde{u})\Phi\tilde{u} = \Phi^T b\ . \tag{4.2}$$

Again, the evaluation of the reduced mass matrix $\Phi^T M(\Phi\tilde{u})\Phi$ and of the reduced stiffness matrix $\Phi^T K(\Phi\tilde{u})\Phi$ is critical for the performance of the reduced model. As long as no phase change happens in any of the patches, the reduced matrices remain constant as well. In contrast to the full model we now collect the changes of the element matrices $\triangle M_{ei}$ and $\triangle K_{ei}$ of all patches undergoing a phase change and build the complete change matrices $\triangle M = M(t_{i+1}) - M(t_i)$ and $\triangle K = K(t_{i+1}) - K(t_i)$, which then can be reduced with the POD basis and added to the reduced systems , i.e.,

$$\Phi^T M(t_{i+1})\Phi = \Phi^T M(t_i)\Phi + \Phi^T \triangle M\Phi,$$
$$\Phi^T K(t_{i+1})\Phi = \Phi^T K(t_i)\Phi + \Phi^T \triangle K\Phi.$$

In Figure 10 one finds the first four POD modes. The eigenvalues of the correlation matrix depicted in Figure 11(a) suggest again a good approximation property of the reduced POD model, which is indeed the fact as can be seen from error plot in Figure 11(b). Already less than 30 modes are sufficient to get adequate results, which is a significant reduction compared to the original number of degrees of freedom.

4.2 Sensitivities and Robustness

Again, we are interested in the robustness of the reduced model with respect to changes in the data. First, we use a different boundary temperature for the generation of the snapshots, which leads to a larger error in the reduced POD model (see Figure 12(a)). But still approximately 50 POD modes are sufficient to get reliable results. Second, we shorten the training time, which has a larger influence on the error as can be seen from Figure 12(b). Here, we need ca. 150 modes to get still a tolerable error.

5 Conclusions

We presented a model reduction approach for free boundary value problems based on the method of snapshot POD. The numerical studies suggest that either a moving mesh approach or a fixed grid approach for the generation of the snapshots guarantees a good approximation property and a robust behaviour of the surrogate model.

References

[1] U. Becker, B. Simeon, and M. Burger. On Rosenbrock methods for the time integration of nearly incompressible materials and their usage for nonlinear model reduction. *Journal of Computational and Applied Mathematics*, 262:333 – 345, 2014.

[2] J. A. Atwell and B. B. King. Reduced order controllers for spatially distributed systems via proper orthogonal decomposition. In *SIAM J. Sci. Comput*, 1999.

[3] N. Aubry, P. Holmes, J. L. Lumley, and E. Stone. The dynamics of coherent structures in the wall region of a turbulent boundary layer. *Journal of Fluid Mechanics*, 192:115–173, July 1988.

[4] C. A. Beattie, J. Borggaard, S. Gugercin, and T. Iliescu. A Domain Decomposition Approach to POD. *Proceedings of the 45th IEEE Conference on Decision and Control*, pages 6750–6756, 2006.

[5] V. Buljak. *Inverse Analyses with Model Reduction: Proper Orthogonal Decomposition in Structural Mechanics*. Computational Fluid and Solid Mechanics. Springer, 2011.

[6] C. C. Cryer. *Free and Moving Boundary Problems*, volume 46. Apr. 1986.

[7] J. F. M. Doren, R. Markovinović, and J.-D. Jansen. Reduced-order optimal control of water flooding using proper orthogonal decomposition. *Computational Geosciences*, 10(1):137–158, May 2006.

[8] M. Gubisch and S. Volkwein. *Proper Orthogonal Decomposition for Linear-Quadratic Optimal Control*. 2013.

[9] S. Herkt, K. Dreßler, and R. Pinnau. Model reduction of nonlinear problems in structural mechanics. Technical Report 175, Berichte des Fraunhofer-Instituts f'ur Techno- und Wirtschaftsmathematik (ITWM Report), 2009.

[10] S. Herkt, M. Hinze, and R. Pinnau. Convergence analysis of galerkin POD for linear second order evolution equations. *ETNA*, 40:321–337, 2013.

[11] M. Hinze, M. Kunkel, A. Steinbrecher, and T. Stykel. Model order reduction of coupled circuit-device systems. *International Journal of Numerical Modelling: Electronic Networks, Devices and Fields*, 25(4):362–377, 2012.

[12] M. Hinze and S. Volkwein. Proper orthogonal decomposition surrogate models for nonlinear dynamical systems: Error estimates and suboptimal control. In P. Benner, D. Sorensen, and V. Mehrmann, editors, *Dimension Reduction of Large-Scale Systems*, volume 45 of *Lecture Notes in Computational Science and Engineering*, pages 261–306. Springer Berlin Heidelberg, 2005.

[13] M. Hinze and S. Volkwein. Error estimates for abstract linearquadratic optimal control problems using proper orthogonal decomposition. *Computational Optimization and Applications*, 39(3):319–345, 2008.

[14] J. Krenciszek. *Proper Orthogonal Decomposition for Contact and Free Boundary Problems*. PhD thesis, TU Kaiserslautern, 2014.

[15] P. Krysl, S. Lall, and J. E. Marsden. Dimensional model reduction in non-linear finite element dynamics of solids and structures. *International Journal for Numerical Methods in Engineering*, 51:479–504, 2000.

[16] K. Kunisch and S. Volkwein. Galerkin proper orthogonal decomposition methods for parabolic problems. *Numerische Mathematik*, 148:117–148, 2001.

[17] K. Kunisch and S. Volkwein. Galerkin proper orthogonal decomposition methods for a general equation in fluid dynamics. *SIAM Journal on Numerical Analysis*, 40(2):492–515, 2010.

[18] S. Lall, P. Krysl, and J. E. Marsden. Structure-preserving model reduction for mechanical systems. *Physica D: Nonlinear Phenomena*, 184(1-4):304–318, Oct. 2003.

[19] W. D. Murray and F. Landis. Numerical and machine solutions of transient heat-conduction problems involving melting or freezing. *Journal of Heat Transfer*, 81:875–898, 1990.

[20] A. K. Pani and P. C. Das. A Finite Element Galerkin Method for a Unidimensional Single-Phase Nonlinear Stefan Problem with Dirichlet Boundary Conditions. *IMA Journal of Numerical Analysis*, 11(1):99–113, 1991.

[21] R. Pinnau. Model reduction via proper orthogonal decomposition. In W. Schilders, H. Vorst, and J. Rommes, editors, *Model Order Reduction: Theory, Research Aspects and Applications*, volume 13 of *Mathematics in Industry*, pages 95–109. Springer Berlin Heidelberg, 2008.

[22] C. W. Rowley. Model Reduction for Fluids, Using Balanced Proper Orthogonal Decomposition. *International Journal of Bifurcation and Chaos*, 15(03):997–1013, Mar. 2005.

[23] A. Verhoeven, M. Striebel, J. Rommes, E. Maten, and T. Bechtold. Proper orthogonal decomposition model order reduction of nonlinear IC models. In A. D. Fitt, J. Norbury, H. Ockendon, and E. Wilson, editors, *Progress in Industrial Mathematics at ECMI 2008*, Mathematics in Industry, pages 441–446. Springer Berlin Heidelberg, 2010.

[24] S. Volkwein. Optimal control of a phase-field model using proper orthogonal decomposition. *ZAMM*, 81(2):83–97, 2001.

[25] V. R. Voller and C. R. Swaminathan. Fixed grid techniques for phase change problems: a review. *International Journal*, 30:875–898, 1990.

[26] S. Walton, O. Hassan, and K. Morgan. Reduced order modelling for unsteady fluid flow using proper orthogonal decomposition and radial basis functions. *Applied Mathematical Modelling*, 37(20-21):8930–8945, Nov. 2013.

[27] J. Weller, E. Lombardi, and M. Bergmann. Numerical methods for low-order modeling of fluid flows based on POD. *MC2 - INRIA Bordeaux - Sud-Ouest , Institut de Mathématiques de Bordeaux - IMB*, 2008.

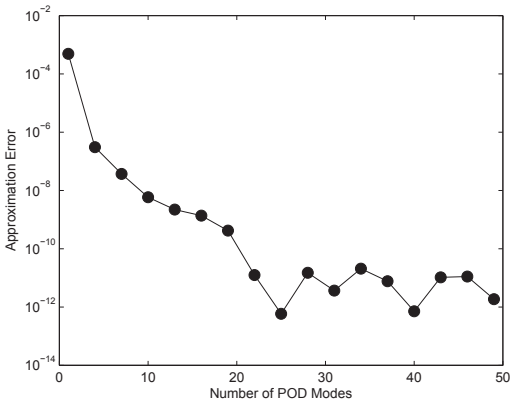

(a) Landau-type transformation ($\kappa = 0.01, T_0 = 20$)

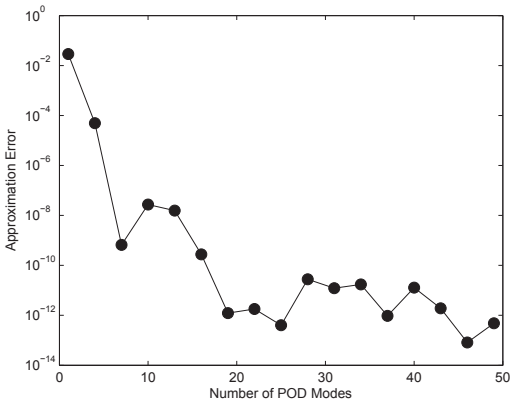

(b) Landau-type transformation ($\kappa = 1, T_0 = 5$)

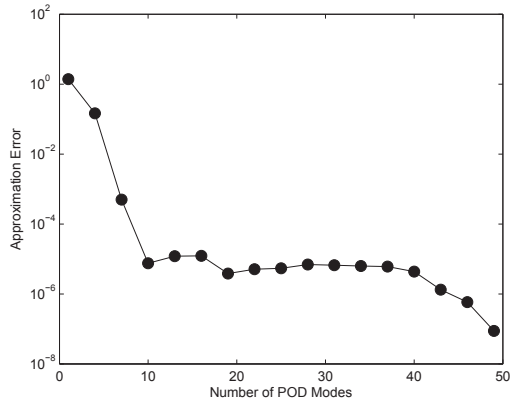

(c) Control Volume ($\kappa = 0.01, T_0 = 20$)

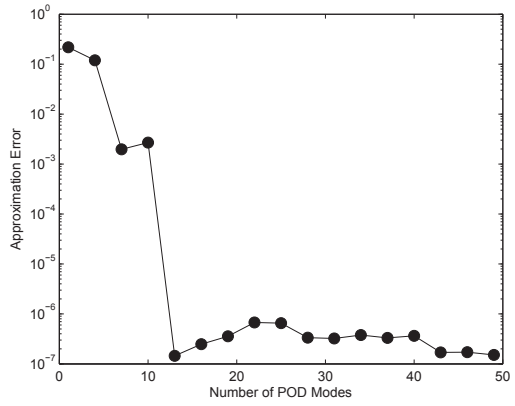

(d) Control Volume ($\kappa = 1, T_0 = 5$)

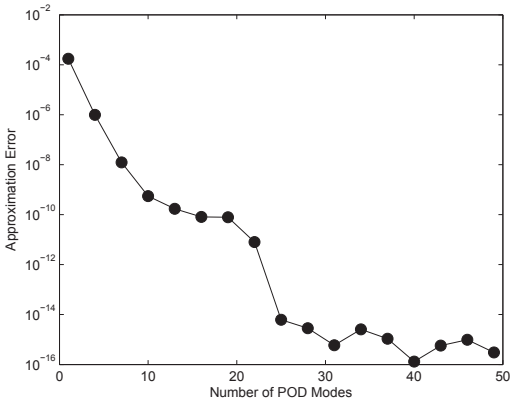

(e) Moving Mesh ($\kappa = 0.01, T_0 = 20$)

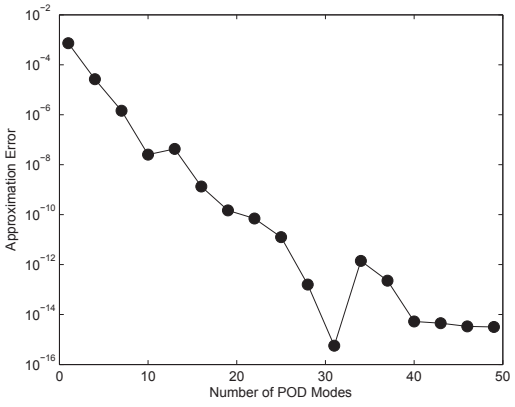

(f) Moving Mesh ($\kappa = 1, T_0 = 5$)

Figure 6: Approximation error of the reduced POD model for $\kappa = 0.01$ (left) and $\kappa = 1$ (right)

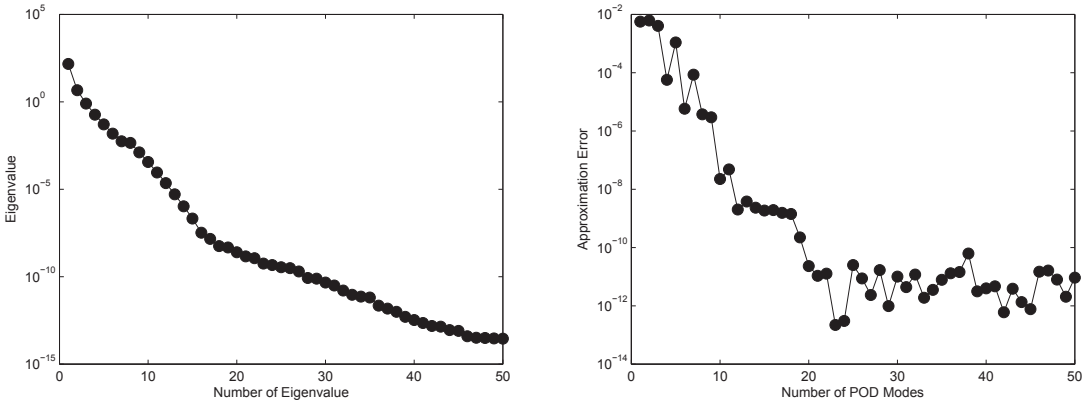

(a) Eigenvalues of the correlation matrix

(b) Landau-type transformation

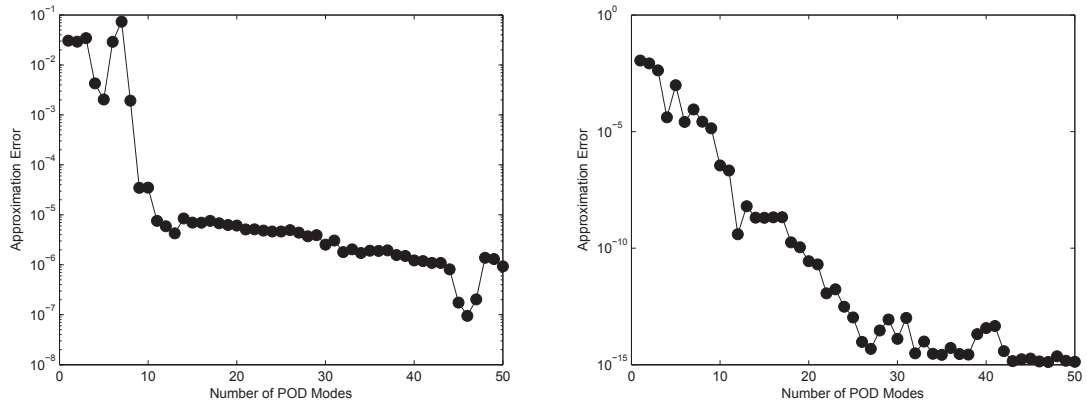

(c) Control Volume

(d) Moving Mesh

Figure 7: Approximation error of the POD reduced systems generated with $T_0 = 1$ and then simulated until $T_0 = 20$

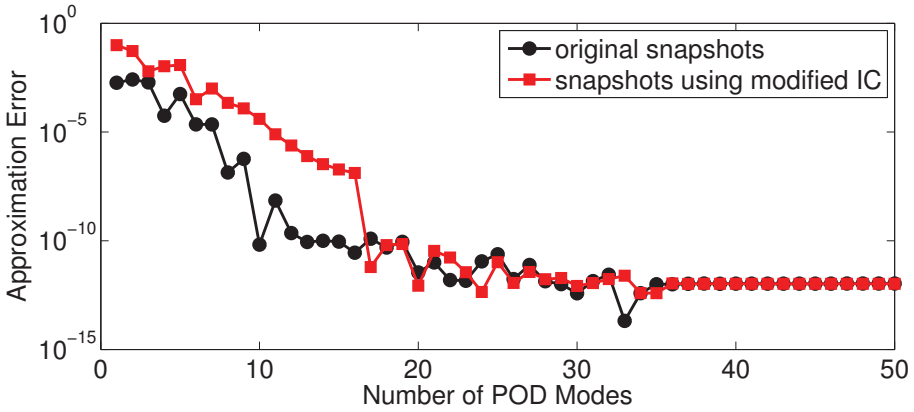

(a) Eigenvalues of the correlation matrix

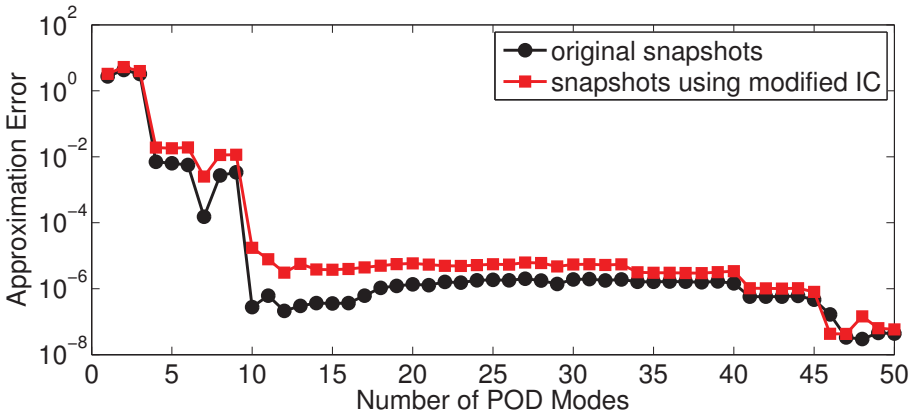

(b) Landau-type transformation

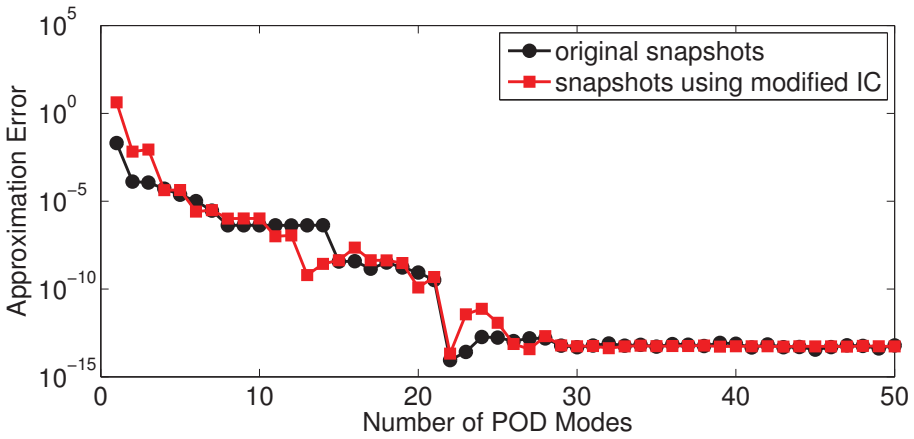

(c) Control Volume

Figure 8: Approximation error of the reduced POD model with modified initial condition

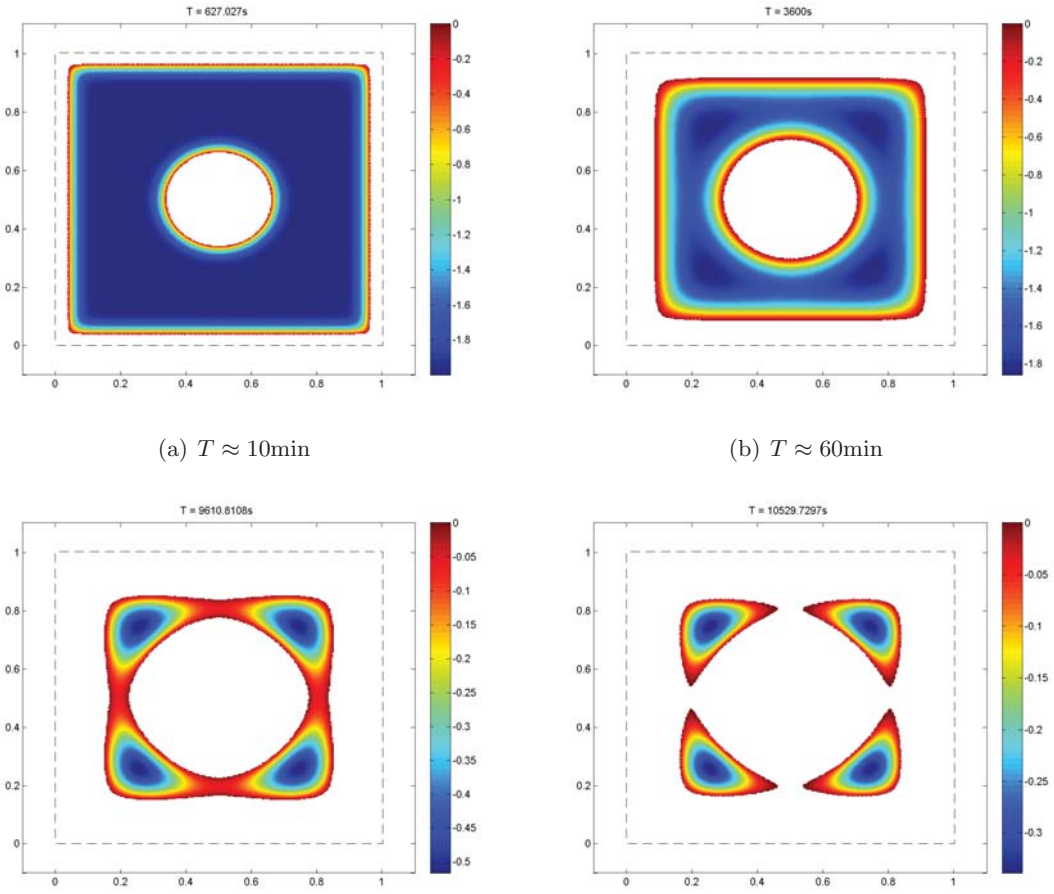

(a) $T \approx 10$min

(b) $T \approx 60$min

(c) $T \approx 160$min

(d) $T \approx 175$min

Figure 9: Solution of the 2d two-phase Stefan problem (solid part)

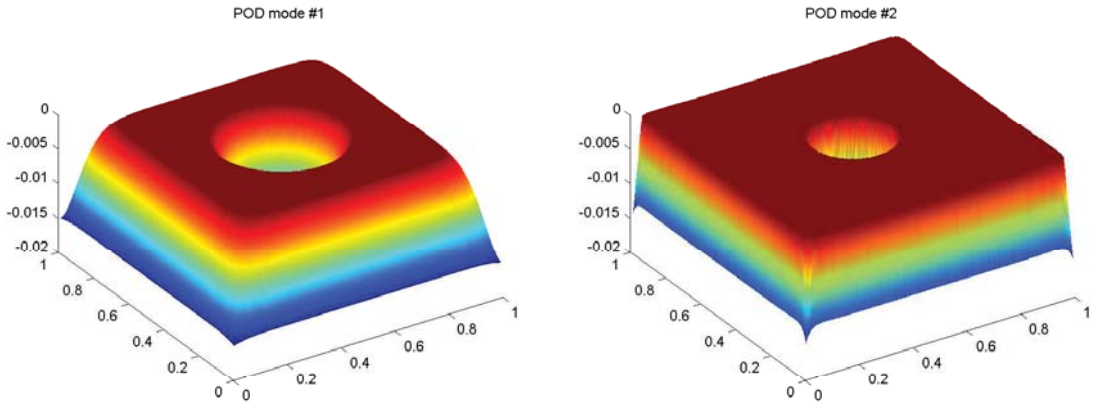

(a) POD mode 1

(b) POD mode 2

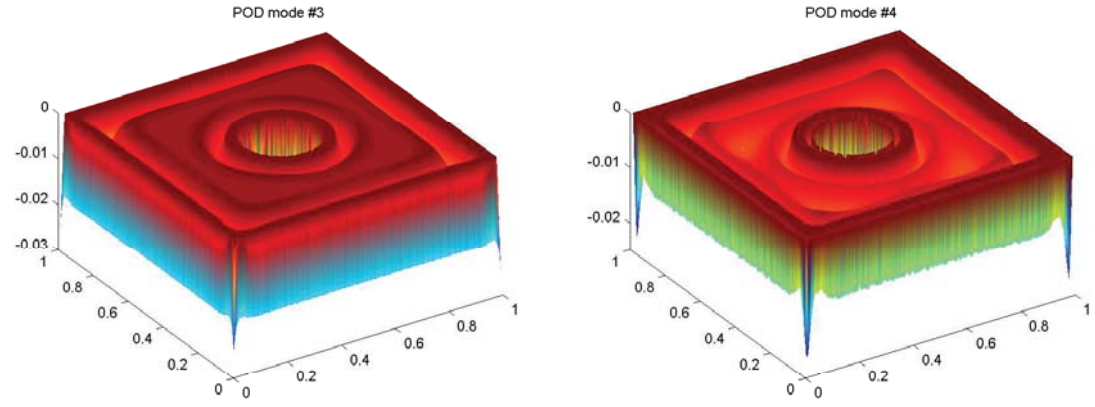

(c) POD mode 3

(d) POD mode 4

Figure 10: The first 4 POD modes (without boundary values)

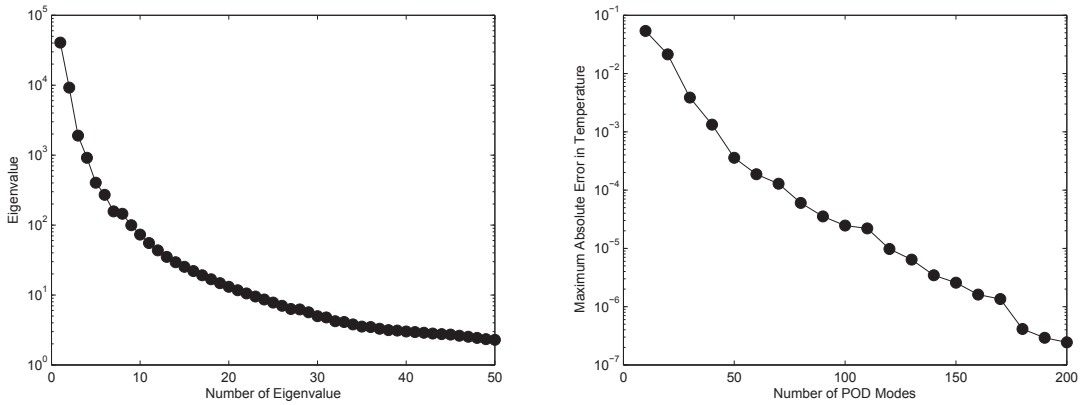

(a) Eigenvalues of the correlation matrix

(b) Original Snapshots

Figure 11: Maximum Error in the Temperature of Reduced POD Model

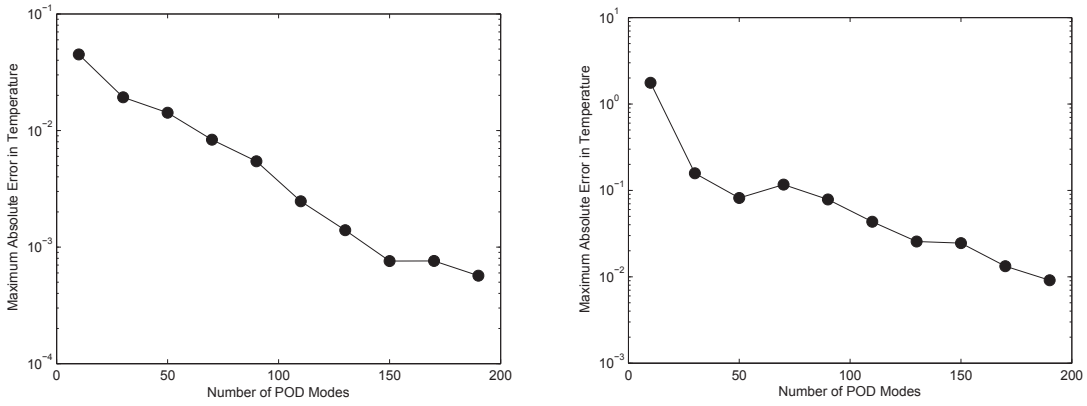

(a) Snapshots generated with 30 °C ambient temperature (20 °C in the original system)

(b) Snapshots from the first half of the time interval

Figure 12: Maximum Error in Temperature of the Reduced POD Model